

Electromagnet Gripping in Iron Foundry Automation Part II: Simulation

Rhythm-Suren Wadhwa

Department of Production and Quality Engineering, NTNU
Trondheim, 7051, Norway

Abstract

This paper compares the simulation and initial experimental results for robust part handling by radially symmetric cylindrical electromagnetic gripper heads, that are used in foundry manufacturing assembly operation. Knowledge of the direct holding force is essential to determine if a given electromagnet is capable of preventing part slipping during pick and place operation. Energy based model and the magnetic circuit model have been described. The latter is developed further and compared with results from a FEA software. It was found that the magnetic circuit model, although simple in form, was limited in its ability to accurately predict the holding force over the entire range of conditions investigated. The shortcomings in the model were attributed to its inability to accurately model the leakage flux and non-uniform distribution of the magnetic flux. A finite element allowed for the ability to couple the mechanical and magnetic models. The finite element model was used to predict the magnetic field based off the solutions to the mechanical (σ) and the magnetic model (B).

Keywords: Foundry Automation, Handling Electromagnet Design

1. Introduction

Robot grippers are used to position and retain parts in an automated assembly operation. Electromagnet grippers offer simple compact construction with no moving parts, uncomplicated energy supply, flexibility in holding complex parts and reduced number of set-ups, and are thus suitable to ferrous metalcasted parts. However, their use is limited to ferrous materials (Iron, Nickel, Cobalt), electromagnet size is directly dependant on required prehension force; residual magnetism in the part when handled when using DC supplies requires the additional of a demagnetizing operation to the manufacturing process. Smart materials, commonly classified according to their energy transduction mode as piezo-electrics, shape memory alloys, and magnetostrictives, have been shown to be useful in low bandwidth application, and micro gripping applications, but they still have limitations in a high volume manufacturing environment [1].

An electromagnet consists of at least one pair of north and south magnetic poles that are separated by an airgap. In

this way, there is practically no magnetic field present when a current flows through the coil, because air presents a very high reluctance to the magnetic flux. When a part is placed on the surface of the electromagnet in such a way that it connects a north and south pole, the magnetic flux can be established, given that the part is made of a ferromagnetic material. The magnetic flux will produce a force of attraction between the part and the electromagnet, as mentioned in the previous section. Two parts made of the same material and having the same geometry and dimensions could experience a different force of attraction on a given electromagnet if the contact conditions between the workpiece and the electromagnet are different for the two of them. Of one of the parts has a rougher surface or has a larger flatness error, the contact interface will have larger airgaps that have to be transversed by the magnetic flux in order to complete the magnetic circuit.

The users of electromagnets in iron foundries know that factors such as material hardness, surface contact conditions, and electromagnet design influence the holding force. Most of the available literature in foundry automation is of a commercial nature [2,3,4]. The author believes that a predictive model for determining the holding force will enable the design of the optimum operating geometry and/or conditions to prevent part slip during robot handling/assembly. Consequently, the need for costly and time intensive experimentation will be minimized.

This paper compares the results from the magnetic circuit model and energy model with available commercial software COMSOL 4.0, for a cylindrical radially symmetrical electromagnet.

2. Modeling Electromagnetic Behavior

Several energy based models have been created in an attempt to capture the non-linear behaviour or electromagnets. Modeling techniques by Dapino et. al [5] include a thermodynamic approach for estimating magnetization to field. Additional modeling techniques have been reported by Sablik and Jiles [6], where internal energy minimization is used to ensure mechanical

equilibrium. Analytical methods have also been developed, but mainly for predicting magnetostrictive performance [7]. When analyzing complex geometries finite element method generally gives more accurate results.

The industrial set-up for the experiments was described in [1], and the following sections, the energy based model, magnetic circuit model and the FEA model used to simulate experimental data are explained. As a basis for comparison, the analytical method for calculating magnetization factor for cylindrical electromagnets is compared to FEA predictions where the effect of airgaps and varying current through the electromagnet coil on the holding force is investigated. Comsol Multiphysics 4.0 magnetostatics (with currents) is the finite element model was used in the research.

To determine the magnetization effect via FEA approach the external field is calculated by determining the magnetic field at a point of interest in space at a certain distance from the magnet, in the absence of the sample part. The magnetization factor was calculated for several aspect ratios, where the thickness of the sample always remained 2-inches. The airgap was varied to change the aspect ratio, and the effect of electromagnet coil heating over a period of 20 minutes (~robot assembly cycle time) was observed.

3. Magnetic Field Distributions

This section analyzes different basic electromagnet setups and their effects on the magnetic properties of a system. Magnetic field distributions will be used for each setup to emphasize key differences between different designs.

As a basis for comparison, the analytical method for calculating the magnetization factor of a cylindrical core is compared to FEA predictions, where the effect of aspect ratio on magnetization is investigated. A COMSOL Multiphysics 4.0 magnetostatic (with currents) finite element model was created with a geometry consisting of a rectangular core immersed in a coil, surrounded by an air domain with dimensions of three times the largest dimension of the rod and coil (Figure 1).

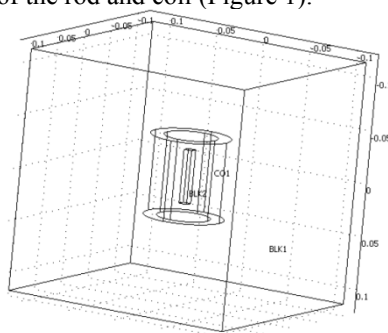


Figure 1: COMSOL Magnetostatics (with currents) geometric rod coil setup.

Equation 1 gives a general expression for determining the effective magnetic field within a sample, with a known value of N_d (magnetization factor) [7]. Since calculation of the effective magnetic field (H_{eff}) requires a knowledge of N_d (geometry dependent), the magnetic field within the sample is normally difficult to calculate (especially for complicated geometries).

$$H_{eff} = H_{ext} - H_d = H_{ext} - N_d M \quad (1)$$

Ellipsoidal geometries have been shown to have a relatively constant magnetic field distribution, leading to one value of magnetization factor for the entire geometry. An analytical expression for calculating the demagnetization factor as a function of a dimensional ratio (k) was developed by [8] (Equation 2). The dimensional ratio, k, is determined by dividing the length of the semimajor axis by the semiminor axis.

$$N_d = \frac{1}{k^2 - 1} \left[\frac{k}{\sqrt{k^2 - 1}} \log_e \left(k + \sqrt{k^2 - 1} \right) - 1 \right] \quad (2)$$

It was desired to simulate the magnetic field behavior along the radius and length of the rod. A 2D axisymmetric, magnetostatics (with currents) model was utilized. The rod was placed at the $r = 0$ location and was surrounded by a coil. The rod and coil setup is surrounded by an air domain ($\mu R = 1$) with dimensions that are three times the length of the coil, which is the largest component of the circuit. A current density of $3e6$ A/m² was assigned to the geometry corresponding to the coil. A relative permeability of 50 was assigned to the rod for the experiment.

Figure 2 shows a 2D axisymmetric streamline of the magnetic field when the magnetic sample ($\mu R = 50$) is placed inside the coil. It is evident that due to the demagnetization effect, the magnetic field leaks throughout the length of the rod (i.e., some streamlines fail to travel the full distance of the sample). However, if a magnetic circuit is incorporated into the design of the transducer, then the flux leakage can be drastically reduced. In Figure 3, a steel flux return path is added to the same setup as in Figure 2, with $\mu R = 2000$ for the steel. The use of a well defined magnetic circuit will allow for the full use of the material capabilities, as there is negligible field lost due to flux leakage.

Rods having a radius of 0.25-inches were analyzed for aspect ratios of 1, 2, and 4 (0.5, 1, and 2-inch long rods respectively). The magnetic rod is assumed to have a

constant permeability of 50. The steel flux return path discussed in the second case has a permeability of 2000. The current density used here is $3e6$ A/m² for all cases.

First, the magnetic field distribution was studied for the no steel flux return case. The radial magnetic field distribution (at the mid-height of the rod) was studied for the no steel flux return case, for cylindrical rods with aspect ratios of 1, 2, and 4, and all with radii of 0.25-inches. The magnetic field data for each aspect ratio was non-dimensionalized according to its maximum magnetic field value. The radial position was also non-dimensionalized (i.e., max field is one, and outer radius position is one).

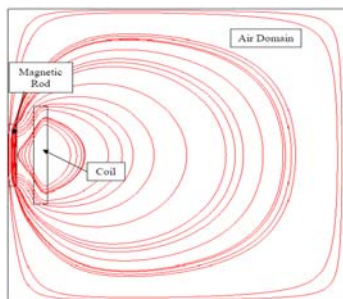


Figure 2: 2D axisymmetric view of magnetic field streamlines showing lines of flux leakage resulting from rod and coil setup.

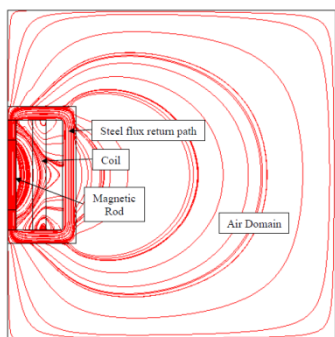


Figure 3: 2D axisymmetric view of magnetic field streamlines showing flux leakage for rod and coil with steel flux return path.

Figure 4 shows the non-dimensional results for the three different aspect ratios. There are two sets of data shown for each aspect ratio. The dashed lines correspond to rods with length and width of half the sample shown by the red lines. Using these dimensions gives the same aspect ratio. It is evident that the non-dimensional magnetic field distribution does not vary for rods of the same aspect ratio. It is important to note that this is only true when comparing magnetic field distributions of the same shape. Also, these distributions are unique to the specific coil design and applied current density. Further, Figure 4 shows that lower aspect ratio samples experience a larger amount of non-dimensional magnetic field leakage from

their centerline to the outer radius. Additionally, it is evident that the magnetic field increases from the center of the rod and reaches a maximum at the end of the rod for all aspect ratio cases. It should also be noted that the relationships shown in Figure 4 are parabolic. This parabolic magnetic field behavior plays a key role in the element type that is chosen for the mesh.

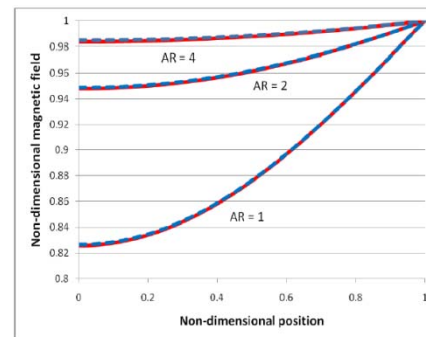


Figure 4: Nondimensional radial magnetic field versus non dimensional position for a rod and coil setup with varying aspect ratios. The dashed lines show rods with different dimensions that yield the same dimensions as the rods shown in the solid lines. All data is normalized to its respective maximum magnetic field.

Next, the magnetic field distribution along the length of the rod was studied for the no steel flux return case, for cylindrical rods with aspect ratios of 1, 2, and 4, and all with radii of 0.25-inches. Again, the magnetic field data for each aspect ratio was non-dimensionalized according to its maximum value. The magnetic field behaviour described in the above two cases is summarized in Table 1. As the aspect ratio is increased, the percentage difference between the maximum and minimum magnetic field through different locations along the radial span decreases. On the contrary, the percentage difference between maximum and minimum magnetic field along the length increases for samples with higher aspect ratio ratios. Differences in magnetic field of 80.9% were seen along the length of a 2-inch, 0.25-inch diameter sample.

Aspect ratio	% difference in magnetic field along radius	% difference in magnetic field along length
1	17.4	54
2	5.2	70
4	1.6	80.9

Table 1. Percentage difference of magnetic field along radius and length of cylindrical samples with radii of 0.25-inches and lengths of 0.5, 1, and 2-inches (aspect ratio ratios of 1, 2, and 4) for rod and coil setup.

The radial magnetic field distribution (at the mid-height of the rod) was studied for the steel flux return case, for the same cases as done for the no steel flux return path studies. It was clear that the presence of the steel flux return path increases the magnetic field within the sample, as well as

creates a more uniform distribution of magnetic field. Table 2 summarizes the magnetic field behavior. It can be observed that as the aspect ratio increases, the percentage difference between the maximum and minimum magnetic field through the radial span decreases. In contrast, the percentage difference between maximum and minimum magnetic field along the length increases for samples with higher aspect ratios. Differences in magnetic field of 6.5% were seen along the length of a 2-inch, 0.25-inch diameter sample. However, in comparison to Table 1, the steel flux return path eliminates a large amount of the flux leakage leading to small percentage differences in magnetic field along the radius and length of the sample.

aspect ratio	% difference in magnetic field along radius	% difference in magnetic field along length
1	0.9	0.7
2	0.6	3
4	0.2	6.5

Table 2. Percentage difference of magnetic field along radius and length of cylindrical samples with radii of 0.25-inches and lengths of 0.5, 1, and 2-inches (aspect ratios of 1, 2, and 4) for rod, coil, and steel flux return path.

It was clear that the spatial variation of magnetic field varies greatly with the setup. The above parametric study suggested that it is important to include a flux return path. It was also found that it is desirable to use samples of lower aspect ratio, as the percentage change in magnetic field is much smaller for lower aspect ratio samples. Seeing these, the magnetic circuit was modeled before experimentation.

4. Magnetic Models

Energy Based Model

In the magnetic field, the energy associated with the system is distributed throughout the space occupied by the field. Assuming no losses, the energy stored in the system per unit volume when increasing the flux density from zero to B is:

$$W_f = \int_0^B HdB \quad (3)$$

From this expression, a relation for the mechanical force can be obtained by the method of energy or coenergy. These two methods are derived from the principle of conservation of energy and are very well documented in the literature such as Sen 1989, Fitzgerald 1985. The expression for the force obtained with the energy method is:

$$F = -\frac{\delta W_m}{\delta x} \quad \lambda = \text{constant} = \frac{B^2 \cdot A}{\mu_0} \quad (4)$$

Where λ is the flux linkage, which is equal to the magnetic flux (ϕ) in the system times the number of turns in the coil (N) generating the magnetic field. It can be seen from Eq. (4) that the stored energy in the magnetic field, and thus the mechanical force, is a function of the magnetic flux (or flux density) present in the system. Thus, the available force for a specific device with a given MMF is determined by the reluctance of the device.

Magnetic Circuit Model

The magnetic circuit approach is an analytical method, analogous to electric circuit analysis, for modeling electromagnetic devices [9,10]. Cherry et al. in a classic paper [11], demonstrated the duality between electric and magnetic circuits. The below Magnetic circuit model was derived in [1].

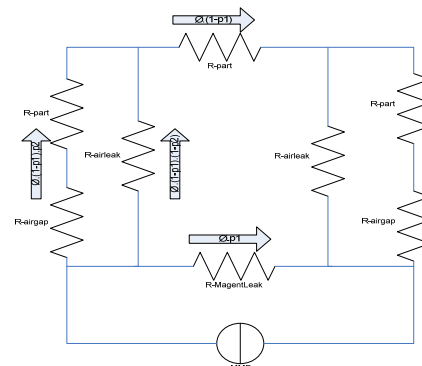


Figure 5: Equivalent Magnetic Circuit of the Magnet-Part System

The results from the above magnetic circuit model were compared with COMSOL FEA model described below.

COMSOL FEA Model

The magnetic model was created using a 2D axisymmetric magnetostatics (with currents) module. The air domain was assigned the dimensions of width and length equal to three times the maximum dimension of the electromagnet. The air and aluminum parts were assigned a $\mu R = 1$, steel casing a $\mu R = 2000$, and the center rod was assigned a variable permeability via $\mu R(B, \sigma)$. The magnetic field is assigned via a current density which has units of current per unit area. The air domain with normal mesh used for this study of a 2D axisymmetric rod and coil setup is shown in Figure 6 there is a tradeoff between computational efficiency and model accuracy, as a finer mesh normally requires more memory and computational time, but generally gives a more accurate solution.

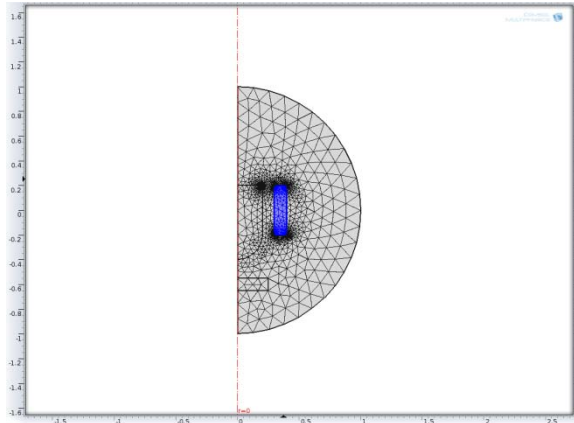


Figure 6: COMSOL model of normal mesh model for radially symmetric electromagnet.

When assigning a mesh to a geometry, one must also define what is known as a shape function. A shape function – linear, quadratic or cubic- defines the relationship between a particular variable. Pian and Lee [12] have shown that the conventional elements such as 3-node triangular and 4-node quadrilateral elements will lead a stiffness matrix with all infinite values. The inability of these elements to give accurate results when dealing with incompressible problems should be considered when selecting a mesh type. The magnetic problem discussed in this research involves the magnetic form of Gauss’s Equation, which employs an incompressibility condition. Considering this, the use of conventional 3-node triangular and 4-node quadrilateral elements when solving magnetostatics problems was avoided.

Other important boundary conditions include axial symmetry and continuity. Axial symmetry is defined for 2D axisymmetric models at $r = 0$, and assumes a symmetric condition such that the properties of the system do not vary azimuthally. The continuity boundary condition enforces continuity of the tangential components of the magnetic field via: $n \times (H_2 - H_1) = 0$. This boundary condition is used at the junction of two different subdomains with different magnetic properties.

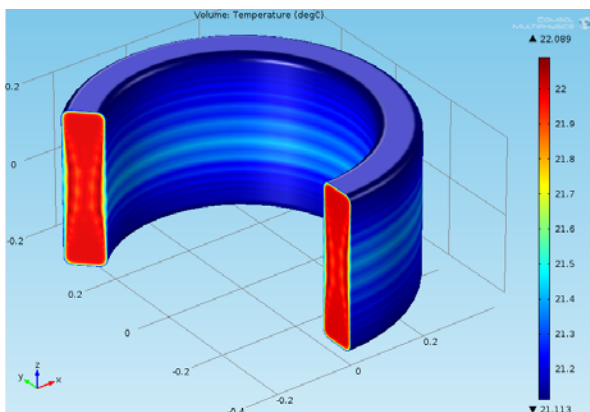


Figure 7: COMSOL model of temperature gradient for radially symmetric electromagnet.

Experimental data was recorded for different magnetic field intensities with varying electromagnet aspect ratios and solenoid currents. The predicted results were within 10% accuracy with the FEA model, when compared to the experiments.

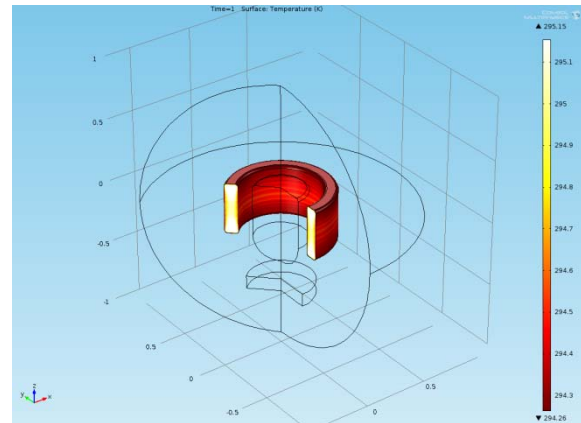


Figure 8: COMSOL model of surface temperature for radially symmetric electromagnet.

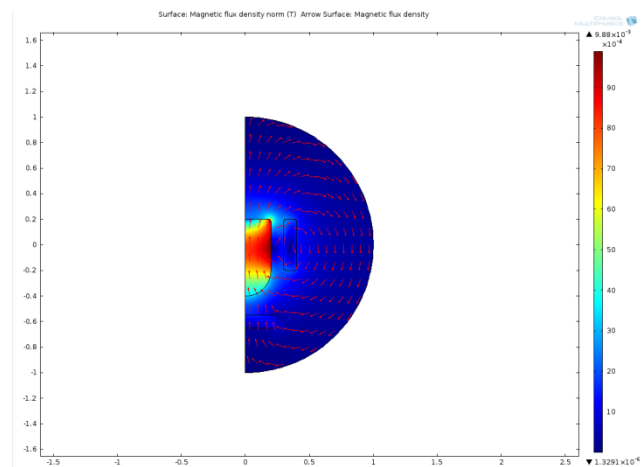


Figure 9: COMSOL model of magnetic flux density for radially symmetric electromagnet.

5. Conclusions and Future Work

It was shown that a steel flux return path greatly reduces the radial and longitudinal variations of field. The part texture attributes (surface roughness and texture) affect the holding forces of an electromagnet gripper. Upcoming effort in this area will present the effect of these attributes on normal and tangential holding forces, and details of the experimental analysis.

6. References

- [1] Wadhwa, R.S., Lien, T. Electromagnet Gripping in Iron Foundry Automation Part I: Principles and Framework , IJCSI, Vol 6, Issue 6, Nov 2011

- [2] Robust Prehension for ferrous metalcasted product families, Proceedings of MITIP 2011
- [3] *Anonymous*, New shelf robot saves vital space in the foundry environment, *The Industrial Robot*. Bedford: 2006. Vol. 33, Iss. 2; p. 145
- [4] *Anonymous*, The Castings Center selects STRIM, Euclid, and Prelude Software, *The Industrial Robot*. Bedford: 1996. Vol. 23, Iss. 6; p. 6
- [5] Wetzel, S. GM's Iron Finishing Automation, *Modern Casting*, 2008; 98,1 ABI/INFORM Complete pg.38
- [5] P. G. Evans, M. J. Dapino, and J. B. Restorff, "Bill Armstrong memorial symposium: free energy model for magnetization and magnetostriction in stressed Galfenol alloys," in *Proceedings of SPIE, Behavior and Mechanics of Multifunctional and Composite Materials*, San Diego, CA, 2007, p. p. 652619.
- [6] M. J. Sablik and D. C. Jiles, "Coupled Magnetoelastic Theory of Magnetic and Magnetostrictive Hysteresis," *Ieee Transactions on Magnetism*, vol. 29,no. 4, pp. 2113-2123, Jul 1993.
- [7] J. Atulasimha, "Characterization and Modeling of the Magnetomechanical Behavior of Iron-Gallium Alloys," Phd Dissertation *Department of Aerospace Engineering*, MD, 2006.
- [8] S. Chikazumi, *Physics of Magnetism*: John Wiley and Sons, Inc., 1964.
- [9] Hoole, S.R, *Computer Aided Analysis and Design of Electromagnetic Devices*, 1989
- [10] Law, J.D., Modeling of Field Regulated Reluctance Machines, PhD Thesis, University of Wisconsin-Madison, 1991
- [11] Cherry, E.C.: The duality between interlinked electric and magnetic circuits and the formation of transformer equivalent circuits, *Proc. Phys. Soc.*, 1949, 62, p.101
- [12] T. H. H. Pian and S. W. Lee, "Finite-Elements for Nearly Incompressible Materials," *Aiaa Journal*, vol. 14, no. 6, pp. 824-826, 1976.

Acknowledgments

Financial support from the AutoCast Consortium and the Norwegian Research Council is gratefully acknowledged.

First Author Rhythm Suren Wadhwa is a PhD student at the department of production and quality engineering, NTNU. She has worked in the Manufacturing Automation industry for five years. Current research interests include assembly automation, optimization techniques, assembly simulation and industrial robotics. She was the president of Society of Women Engineers at the University of Michigan. She has a Masters Degree in Mechanical Engineering from University of Michigan, and Bachelors degree in Manufacturing Processes Automation Engineering.